Materials Today Bio 13 (2022) 100211

Contents lists available at ScienceDirect

Materials Today Bio

journal homepage: www.journals.elsevier.com/materials-today-bio

A multifunctional ATP-generating system by reduced graphene oxide-based scaffold repairs neuronal injury by improving mitochondrial function and restoring bioelectricity conduction

Huiquan Jiang [a,b], Xu Wang [b], Xiao Li [a,b], Yi Jin [c], Zhiwen Yan [b], Xiangyun Yao [b], Wei-En Yuan [c,***], Yun Qian [b,**], Yuanming Ouyang [b,*]

[a] College of Fisheries and Life Science, Shanghai Ocean University, Shanghai, China
[b] Department of Orthopedics, Shanghai Jiao Tong University Affiliated Sixth People's Hospital, Shanghai, China
[c] Engineering Research Center of Cell & Therapeutic Antibody, Ministry of Education, School of Pharmacy, Shanghai Jiao Tong University, Shanghai, China

ARTICLE INFO

Keywords:
Peripheral nerve injury
Tissue engineering
Nerve guide conduit
Melatonin
Reduced graphene oxide

ABSTRACT

Peripheral nerve injury usually impairs neurological functions. The excessive oxidative stress and disrupted bioelectrical conduction gives rise to a hostile microenvironment and impedes nerve regeneration. Therefore, it is of urgent need to develop tissue engineering products which help alleviate the oxidative insults and restore bioelectrical signals. Melatonin (MLT) is an important endogenous hormone that diminishes the accumulation of reactive oxygen species. Reduced graphene oxide (RGO) possesses the excellent electrical conductivity and biocompatibility. In this study, a multilayered MLT/RGO/Polycaprolactone (PCL) composite scaffold was fabricated with beaded nanostructures to improve cell attachment and proliferation. It also exhibited stable mechanical properties by high elastic modulus and guaranteed structural integrity for nerve regeneration. The live/dead cell staining and cell counting kit assay were performed to evaluate the toxicity of the scaffold. JC-1 staining was carried out to assess the mitochondrial potential. The composite scaffold provided a biocompatible interface for cell viability and improved ATP production for energy supply. The scaffold improved the sensory and locomotor function recovery by walking track analysis and electrophysiological evaluation, reduced Schwann cell apoptosis and increased its proliferation. It further stimulated myelination and axonal outgrowth by enhancing S100β, myelin basic protein, β3-tubulin, and GAP43 levels. The findings demonstrated functional and morphological recovery by this biomimetic scaffold and indicated its potential for translational application.

1. Introduction

Peripheral nerve defect is usually caused by traumatic accidents as a huge clinical challenge. The autologous nerve transplantation is the gold standard applied for long defects of nerve tissue, especially when the direct end-to-end suture is not suitable [1]. The primary disadvantage of autograft transplantation is the loss of function in the donor site and the limitation of donor tissue [2–4]. Nerve tissue engineering scaffolds are under rapid development to promote peripheral nerve regeneration as a type of promising alternative therapy [5].

Nerve guide conduit (NGC), an artificial nerve scaffold, can bridge the nerve stumps between two nerve ends [6,7]. A variety of biomaterials approved by US Food and Drug Administration (FDA) have been fabricated into commercial NGCs [8,9]. Polycaprolactone (PCL) is one of the most available polymers approved by FDA and has been widely applied as substrate material of NGC [10,11]. The low-cost PCL has been widely used in the tissue engineering because it is chemically inert, rarely causes immune responses to the body, and possesses good biocompatibility and biodegradation [12]. PCL is a kind of synthetic aliphatic polyester that can induce the alignment of Schwann cells (SCs). The fabrication of bionic channels with PCL showed high mechanical strength and stability for axonal regeneration [13]. The PCL fibers were crossed to form highly ordered topological structure through electrospinning. More importantly, suitable porosity in the surface of the PCL scaffold is vital to

* Corresponding author.
** Corresponding author.
*** Corresponding author.
E-mail addresses: yuanweien@sjtu.edu.cn (W.-E. Yuan), lollipopcloudland@foxmail.com (Y. Qian), ouyangyuanming@163.com (Y. Ouyang).

https://doi.org/10.1016/j.mtbio.2022.100211
Received 26 November 2021; Received in revised form 21 January 2022; Accepted 29 January 2022
Available online 31 January 2022

diffusion of nutritional substances and cell migration [14]. Thus, PCL plays an important role in the nerve tissue engineering.

The microenvironment imbalance occurs after peripheral nerve injury [15]. Peripheral nerve microenvironment imbalance results in oxidative stress and bioelectricity signal abnormality [16,17]. Pharmacotherapy is a traditional therapy for peripheral nerve defects. Melatonin (MLT) is a pineal neurohormone, and it regulates the sleep/wake cycle by combining with plasma membrane G-protein-coupled receptors MT1 and MT2 [18–20]. The accumulation of oxidative substances and free radicals is activated by acute inflammation after peripheral nerve injury. MLT has proved to regulate the circadian rhythm, clear free radical as anti-inflammatory and antioxidant bioactive substances when it enters the body fluids [21,22]. Stazi et al. [23] found that MLT could promote peripheral nerve axon regeneration via MT1 receptors [24]. MLT promoted SC migration by activating Wnt/β-catenin signaling pathway, and thus it reduced the apoptosis of SCs [24]. In addition, Qian et al. [25] demonstrated that MLT-based scaffolds reestablished an ideal microenvironment for peripheral nerve regeneration by activating autophagy, thus MLT helped clear the nerve debris and promoted neural proliferation by restoring mitochondrial functions of SCs. A variety of studies reported that MLT inhibited the formation of neuroma and collagen following trauma on peripheral nerves to promote the axon outgrowth and myelination [26]. However, the study it is still unclear if melatonin can promote nerve repair in addition to other bioactive materials, especially nanomaterials to exert synergistic effects on long-range peripheral nerve defects.

Graphene is recognized as a kind of safe, biocompatible, and functional biomedical nanomaterial widely applied for tissue engineering, and it has drawn great attention in recent years [27]. In 2014, Gu et al. [28] reported the construction of graphene nanoparticles for cell growth. Reduced graphene oxide (RGO) is the reduced product of the extremely oxidized graphene derivative, graphene oxide (GO), and RGO possesses better conductivity than GO [29]. Bioelectricity signal is an essential factor in peripheral nerve microenvironment, due to the electroactive property of the nerve tissues and thus the recovery of bioelectricity signal exerts a vital effect on peripheral nerve regeneration [30]. Conductive NGCs demonstrated that accelerated the recovery of bioelectricity, and it induced angiogenesis of peripheral nerves [31]. In addition, PCL loaded with nanoparticles was confirmed to increase biophysical properties of NGCs to better mimic some physical requirements during nerve repair [32,33].

In this study, a functional composite NGC loaded with MLT and RGO was constructed via electrospinning technology. The morphology, hydrophilicity, and mechanical properties of the composite scaffold were measured, and rat Schwann 96 cells (RSC 96) were used to evaluate the biocompatibility, cellular proliferation, and neural differentiation in vitro. The MLT/RGO/PCL NGCs (Scheme 1) were applied to repair a 10 mm sciatic nerve defect in a Sprague Dawley (SD) rat for 8 weeks in vivo. A series of morphology and functional experiments were designed to evaluate the effects of multifunctional antioxidant and electroconductive nerve scaffolds on peripheral nerve regeneration.

2. Experimental section

2.1. Materials

The PCL (30 kDa) was purchased from HENGQIU (Suzhou, China). The MLT was purchased from Sigma-Aldrich (Shanghai, China), and the RGO nanoparticles were purchased from XFNANO (Nanjing, China). DCM was purchased from Aladdin (Shanghai, China), and DMF was purchased from Macklin (Shanghai, China). The RSC 96 were provided by the National Collection of Authenticated Cell Cultures (Shanghai, China). The Fetal Bovine Serum (FBS), penicillin/streptomycin solution, 0.25% Trypsin-EDTA (1x), and Dulbecco's Modified Eagle's Medium (DMEM) with 4.5 g/L D-Glucose were purchased from Gibco (USA). The LIVE/DEAD Cell Imaging Kit was purchased from Thermo Fisher Scientific (USA), the Annexin V-FITC Apoptosis Detection Kit was purchased from Beyotime (China), and the JC-1 Mitochondrial Membrane Potential Assay Kit was purchased from MCE (Shanghai, China). The CCK8 was purchased from Absin (Shanghai, China), and all the antibodies were purchased from Abcam (USA). The 3–0 nylon sutures, 6–0 nylon sutures, and sterile scalpel blades were purchased from Jinhuan Medical (Shanghai, China).

2.2. Fabrication of MLT/RGO/PCL, MLT/PCL, RGO/PCL, and PCL membranes by electrospinning

The 15% (W/V) PCL and 1% (W/W_{PCL}) MLT were dissolved in a

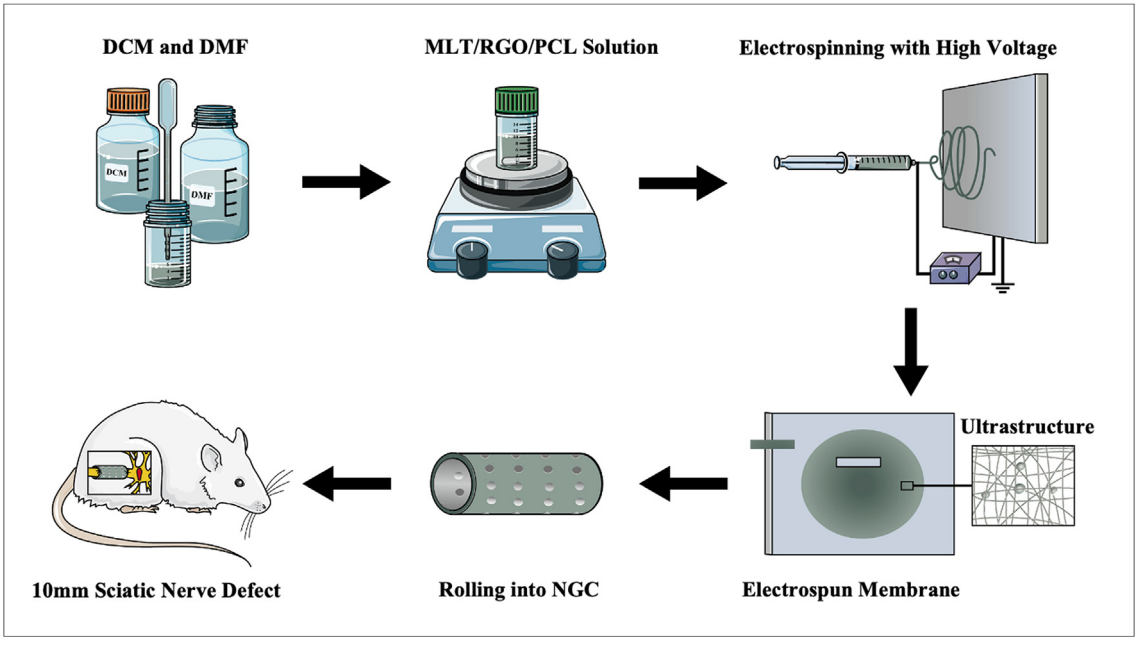

Scheme 1. Schematic diagram of electrospinning NGC and its application for sciatic nerve long-gap defect.

mixed solution of DCM and DMF (7:3, V/V), and 1% (W/W_{PCL}) RGO nanoparticles were added to disperse to the mixed solution after 10 min ultrasonic. A 10 mL injector with a 20G diameter was used to fabricate the membranes in the electrospinning machine (Dongwen High Voltage Power Supply Plant, Tianjin, China) at 1 mL h^{-1}. The eligible membranes were fabricated under 12 kV high voltage and −4 kV low voltage. The membranes were placed dry and avoided light. The 12 × 150 mm electrospun membranes were rolled into NGCs with 2.6 mm inside diameter.

Characterization, Hydrophilicity, Electrical Conductivity, and Mechanical Properties of Electrospun Membranes: SEM (Sirion 200, USA) was used to observe the characteristics of electrospun membranes and NGCs. The membranes with metal spraying were measured under the voltage of 15 kV. The surface and cross-section of NGCs were also measured through SEM. The hydrophilicity of electrospun membranes was measured by Contact Angle Meter (DSA100, German) through the angle formed between the water droplets and membranes. The electrical conductivity of MLT/RGO/PCL scaffolds was evaluated by a three-electrode system (CHI660D, China) at room temperature. The mechanical properties of NGCs were measured by the universal material testing machine (Zwick/Roell Z020, German).

2.3. Cell viability and proliferation assay

RSC 96 were cultured in DMEM with 4.5 g/L D-Glucose, 10% FBS, and 1% penicillin/streptomycin solution at 37 °C with 5% CO_2. 2 × 10^4 RSC 96 were cultured on the MLT/RGO/PCL, RGO/PCL, MLT/PCL, and PCL membranes with germfree. The adhesion and viability of RSC 96 were measured by LIVE/DEAD Cell Imaging Kit, Annexin V-FITC Apoptosis Detection Kit, and JC-1 Mitochondrial Membrane Potential Assay Kit. The stained cells were observed by Confocal Laser Scanning Microscope (Senterra R200-L, German) and analyzed by Image J 1.48 (USA). The Proliferation of RSC96 was measured by CCk8 after 1, 3, 5, and 7 days, and the OD_{450} of culture solution showed the result.

2.4. Cell protein and mRNA level assay

Western Blotting was used to measure the relative protein level of RSC 96 that cultured with electrospun membranes for 4 days. The total proteins were collected and transferred onto PVDF membranes. And the samples were incubated at 4 °C overnight with several primary antibodies, anti-S100β (1:2000, Abcam, USA), anti-MBP (1:5000, Abcam, USA), anti-β3-Tubulin (1:1000, Abcam, USA), anti-GAP43 (1:1000, Abcam, USA), anti-Ki67 (1:5000, Abcam, USA), and GFAP (1:8000, Abcam, USA). Real-time PCR (qPCR) was used to measure the relative mRNA level of RSC 96 that cultured with electrospun membranes for 4 days. The total RNA was collected by TRIzol. (Thermo Fisher Scientific, USA). RNA was then reverse-transcribed into cDNA and run on a real-time PCR biosystem (Applied Biosystems, USA). The primer sequences were S100β (Forward (5′–3′) ATGGTTGCCCTCATTGATGTCTTCC, Reverse (5′–3′) ACCACTTCCTGCTCTTTGATTTCCTC), MBP (Forward (5′–3′) TCTGGAAAGCGAGAATTAGCATCTGAG, Reverse (5′–3′) ACTGTCTTCTGAGGCGGTCTGAG), Ki67 (Forward (5′–3′) GCCAAGAAGACGACTCAAGAGACTG, Reverse (5′–3′) TGTGCCGAAGACTCCTTAAACTCATC), β3-Tubulin (Forward (5′–3′) TGGAGAACACGGATGAGACCTACTG, Reverse (5′–3′) GGTAGCAGACACAAGGTGGTTGAG), GAP43 (Forward (5′–3′) TCTGAGGAGAAGAAGGGCGAAGG, Reverse (5′–3′) AGGACGGCGAGTTATCAGTGGTAG), and GAPDH (Forward (5′–3′) TCGTGGAGTCTACTGGCGTCTT, Reverse (5′–3′) AGGGAGTTGTCATATTTCTCGTGGTTC).

2.5. Animal surgery

The 25 male SD rats, weighing from 200 to 250 g, were placed at the SPF (Specific Pathogen Free) level Laboratory Animal Room of Shanghai Jiao Tong University. At random, these rats were divided into 5 surgical groups, including autograft (5 rats), PCL (5 rats), MLT/PCL (5 rats), RGO/PCL (5 rats), and MLT/RGO/PCL (5 rats) groups. These rats were anesthetized with 40 mg kg^{-1} pentobarbital sodium by peritoneal injection. We structured a 10-mm-long sciatic nerve defect in each rat, and we used the above 12-mm-long nerve guide conduit to bridge the damaged nerve. In the autograft group, we reversed the 10-mm-long sciatic nerve dissected by 180° to bridge the damaged sciatic nerves. The 6–0 nylon sutures were used to suture nerve guide conduit and nerve, and 3–0 nylon sutures were used to suture muscle and skin. For infection prevention, we injected 8 × 10^5 units of penicillin into the rats intraperitoneally. These rats were observed for 8 weeks. In this study, the process of animal surgery was in accordance with the aseptic principles strictly, and all animals were performed according to the guidelines approved by the Institutional Animal Care and Use Committee of Shanghai Jiao Tong University (SJTU, No. A2021090-1).

2.6. Functional recovery assay

We evaluated the functional recovery of regenerated sciatic nerve through walking trace analysis at 16 weeks. For recording footprints, the SD rats whose hind feet were painted with gentian violet were allowed to walk on the surface of a white paper. We measured the length from the second toe to the fourth toe (IT), the first toe to the fifth toe (TS), and the heel to the third toe (PL). Normal feet (N) and experimental feet (E) were both recorded. "SFI = 0" means the great function of the sciatic nerves, and "SFI = -100" means entire sciatic nerve function loss. Thus, SFI was a normal number between −100 and 0. SFI = 109.5 (ETS – NTS)/NTS - 38.3 (EPL - NPL)/NPL +13.3 (EIT - NIT)/NIT - 8.8.

2.7. Electrophysiological recovery assay

NCV of the affected side was calculated through the distance and latency between sciatic nerve stumps. At 8 weeks after surgery, these rats were monitored through electrophysiological assessments. For the exposure of the regenerated sciatic nerve, these rats were anesthetized with appropriate pentobarbital sodium intraperitoneally. In the electromyogram room, a needle electrode was implanted on the inside of rats' right gastrocnemius muscle to record electromyography. And we placed bipolar electrodes at proximal and distal regenerated nerves to collect single electrical signals.

2.8. Morphological recovery assay

At 8 weeks after surgery, we excised the 10-mm-long regenerated sciatic nerve and affected gastrocnemius muscle of rats from autograft, PCL, MLT/PCL, RGO/PCL, and MLT/RGO/PCL groups. We cut the regenerated nerves, fixed by 2.5% glutaraldehyde solution for 2 h at 4 °C, into ultrathin 5 μm thick sections. With 80 kV voltage, these samples were used for TEM. Regenerated nerves were also fixed by 4% paraformaldehyde (PA) for 24 h to cut into 10 μm thick sections. Then, the samples were respectively stained with HE for morphological observation. We used the Image-Pro Plus Software to measure the regenerated axon area and number, the thickness of the myelin sheath, and the average myelinated axon diameter. The affected gastrocnemius muscles were stained with the HE, and we selected random fields of view to evaluate the muscle fibers through Image-Pro Plus. Pm is the percentage of muscle fiber area, Am is the area of muscle fibers, and At is the whole area of the field. PM was used to assess the muscle by Pm. Pm = Am/At × 100%.

2.9. Immunofluorescence and immunohistochemistry staining assay

The paraffin-embedded sciatic nerve sections were incubated at 4 °C overnight with the following primary antibodies: anti-S100β (1:100, Abcam, USA), anti-CD-3 (1:150, Abcam, USA), anti-Ki67 (1:500, Abcam, USA), anti-C-caspase-3 (1:100, Abcam, USA), anti-MBP (1:1000, Abcam, USA), anti-β3-Tubulin (1:2000, Abcam, USA), anti-GAP43 (1:100,

Abcam, USA), and DAPI (1:1000, Abcam, USA) was used to stain the nuclei. The results were measured by Fluorescence Microscope and Optical Microscope (Olympus CX33, Japan).

2.10. Statistical analysis

Mean ± s.d. values were determined from more than three independent experiments. To determine the statistical significance, P values were determined by Student's t-test or ANOVA with Bonferroni correction. Prism6 software was used for statistics analysis.

3. Results

3.1. Fabrication and characterization of scaffolds

The functional composed membranes were fabricated by electrospinning in the field with 12 kV high voltage and −4 kV low voltage. The PCL, MLT, and RGO were added into a mixed solution of dichloromethane (DCM) and N, N-dimethylformamide (DMF) to fabricate the electrospun membranes. MLT/PCL, RGO/PCL, and pure PCL electrospun membranes were also fabricated. The surface of electrospun membranes and cross-section of NGCs were observed through scanning electron microscope (SEM), and the stable topology of fibers (Fig. 1A and B, Supplementary Fig. 1) was exhibited. The uniform nanofibers of MLT/RGO/PCL membrane with a similar diameter (124 ± 11 nm) for all membranes for exchange of nutrient substance and cell attachment. The small pieces of these electrospun membranes were rolled into several 10 mm NGCs with a 2.6 mm inner diameter (Fig. 1C).

The electrical conductivity of four scaffolds was evaluated by a three-electrode system. The MLT/RGO/PCL and RGO/PCL scaffolds displayed a relatively high conductivity of 5.38 ± 0.21 × 10^{-4} S/cm and 5.28 ± 0.13 × 10^{-4} S/cm.

The mechanical property of NGC is one of the most significant characteristics to maintain the tube structure for nerve regeneration in vivo. A universal material testing machine (Zwick/Roell Z020, German) was applied for the mechanical properties testing of PCL, MLT/PCL, RGO/PCL, and MLT/RGO/PCL scaffolds. The Young's modulus (Fig. 1D) significantly increased with the addition of RGO nanoparticles ($p < 0.01$), and it verified the increasing mechanical properties of electrospun scaffolds blended with nanoparticles [32]. The ductility of RGO/PCL and MLT/RGO/PCL scaffolds was also significantly superior to the scaffolds without RGO ($p < 0.01$). However, there was no significant improvement of young's modulus with the addition of MLT. Thus, MLT/RGO/PCL and RGO/PCL NGCs possess more potential for peripheral nerve regeneration from the view of mechanical properties.

The hydrophilicity of these scaffolds was tested by Contact Angle Meter (DSA100, German) by measuring the angle formed between the water droplets and membranes (Fig. 1E). PCL as a hydrophobic biomaterial, the average water contact angle of was 129.3 ± 2.0°. The average water contact angle of RGO/PCL scaffolds was 133.4 ± 1.9°, which was significantly higher than PCL ($p < 0.05$). The hydrophilicity of scaffolds increased with the addition of RGO nanoparticles. The average water contact angle of MLT/PCL scaffolds (117.5 ± 1.2°) was significantly lower than PCL ($p < 0.05$). This suggested that the mixture with MLT which was slightly soluble in water increased the hydrophilicity.

3.2. Biocompatibility of scaffolds In vitro

The cell viability of RSC 96 was tested on PCL, MLT/PCL, RGO/PCL, and MLT/RGO/PCL scaffolds. RSC 96 were cultured on these scaffolds mentioned above at the density of 2 × 10^4 cells/cm^2 for 24 h to verify the cytotoxicity of these scaffolds by Live/Dead Cell Imaging Assay Kit (Thermo Fisher Scientific, USA). Live cells were observed as green fluorescence under laser scanning confocal microscopy (TCS SP8 STED 3X,

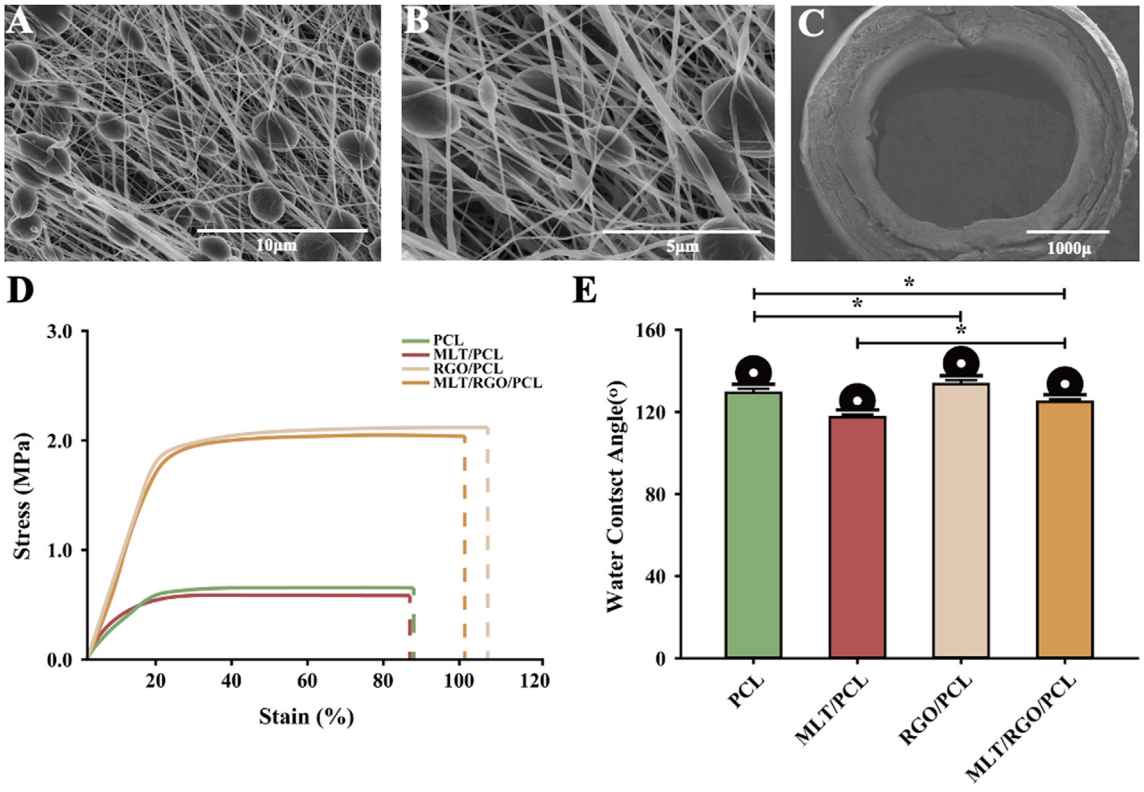

Fig. 1. Characterization, mechanical properties, and hydrophilicity of composite MLT/RGO/PCL scaffolds. (A–B) SEM images of composite MLT/RGO/PCL electrospun membranes by 5.0k × and 10.0k × magnification, respectively. (C) Cross-section SEM image of composite MLT/RGO/PCL conduit by 50x magnification, respectively. (D) Mechanical properties of PCL, MLT/PCL, RGO/PCL and MLT/RGO/PCL, n = 4, mean ± SD. (E) Hydrophilicity of PCL, MLT/PCL, RGO/PCL and MLT/RGO/PCL, n = 5, mean ± SD, *$p < 0.05$.

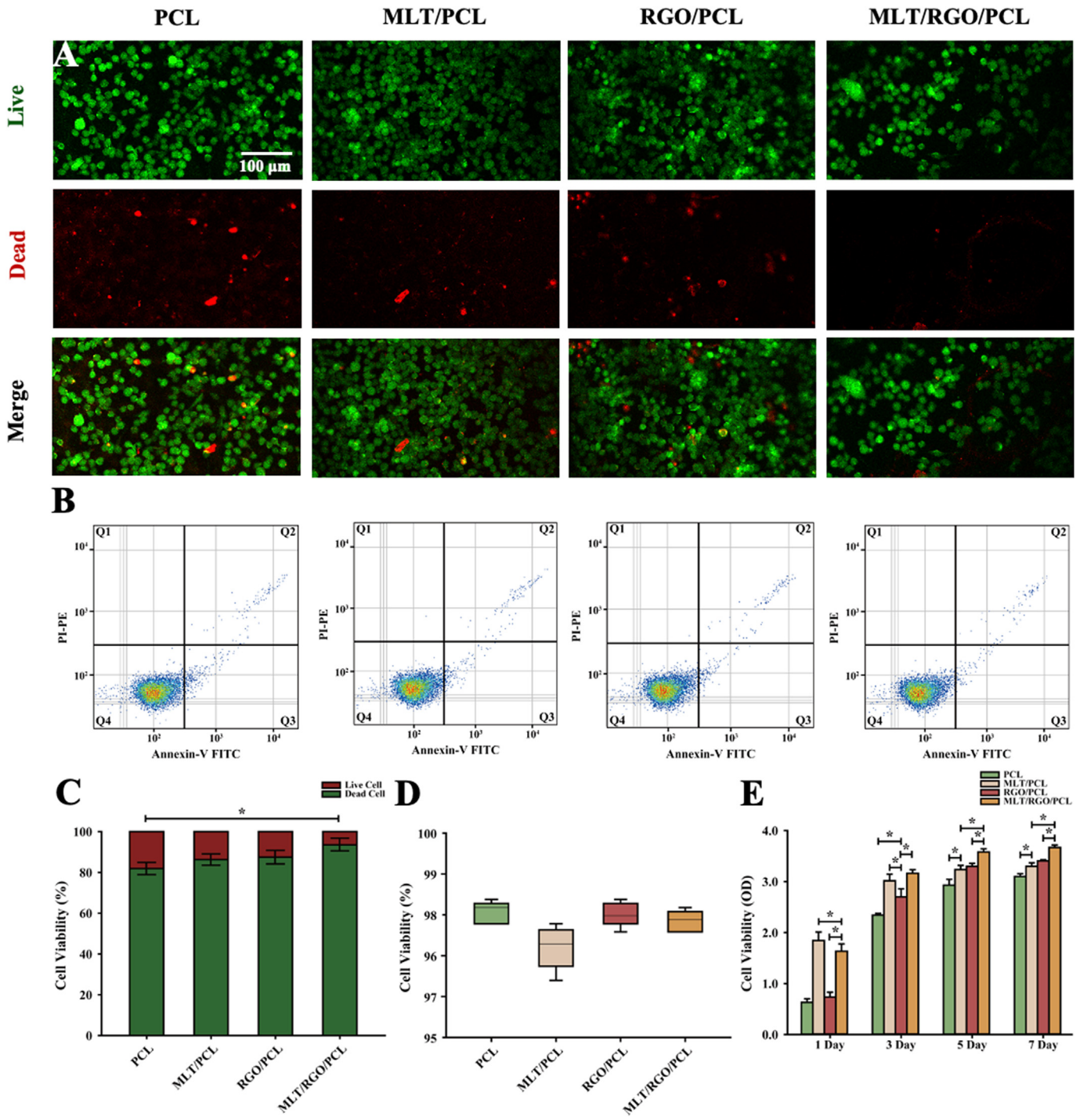

Fig. 2. Cytotoxicity and viability testing in vitro. (A,C) Cytotoxicity of RSC 96 on PCL, MLT/PCL, RGO/PCL, and MLT/RGO/PCL scaffolds by live/dead cell imaging assay. (B,D) Cytotoxicity of RSC 96 on PCL, MLT/PCL, RGO/PCL, and MLT/RGO/PCL scaffolds by Annexin V-FITC apoptosis assay. (E) Cell viability (OD) on PCL, MLT/PCL, RGO/PCL, and MLT/RGO/PCL scaffolds after 1, 3, 5, and 7 days by CCK8 assay, n = 4, *$p < 0.05$.

China), and dead cells were observed as red fluorescence (Fig. 2A). The results showed that these scaffolds loaded with MLT or RGO were nontoxic with cell viability of over 80% (Fig. 2C). The cell viability of RSC 96 on MLT/RGO/PCL scaffolds is 93.8% ± 3.9 that significantly higher than other scaffolds ($p < 0.05$). Thus, the MLT/RGO/PCL composite scaffolds indicated excellent biocompatibility. RSC 96 were cultured on these scaffolds mentioned above at the density of 1×10^5 cells/cm^2 for 24 h to measure cell viability by Annexin V-FITC Apoptosis Detection Kit (Beyotime, China) (Supplementary Fig. 2). Flow Cytometer (Attune CytPix, USA) was used to detect the apoptotic cells with valgus of phosphatidylserine (Fig. 2B). The results showed high cell viability of RSC 96 on all scaffolds with no significant differences ($p > 0.05$) (Fig. 2D).

RSC 96 were then cultured on PCL, MLT/PCL, RGO/PCL, and MLT/RGO/PCL scaffolds at the density of 2×10^4 cells/cm^2 for 1, 3, 5, and 7 days to measure the cell viability and proliferation by Cell Counting Kit-8 (CCK8) (Absin, China). The cell viability of RSC 96 on MLT/PCL, RGO/PCL and MLT/RGO/PCL was significantly higher than PCL scaffolds at different time points ($p < 0.05$) (Fig. 2E). MLT/PCL scaffolds with the release of MLT have higher cell viability than other scaffolds at 1 d ($p <$

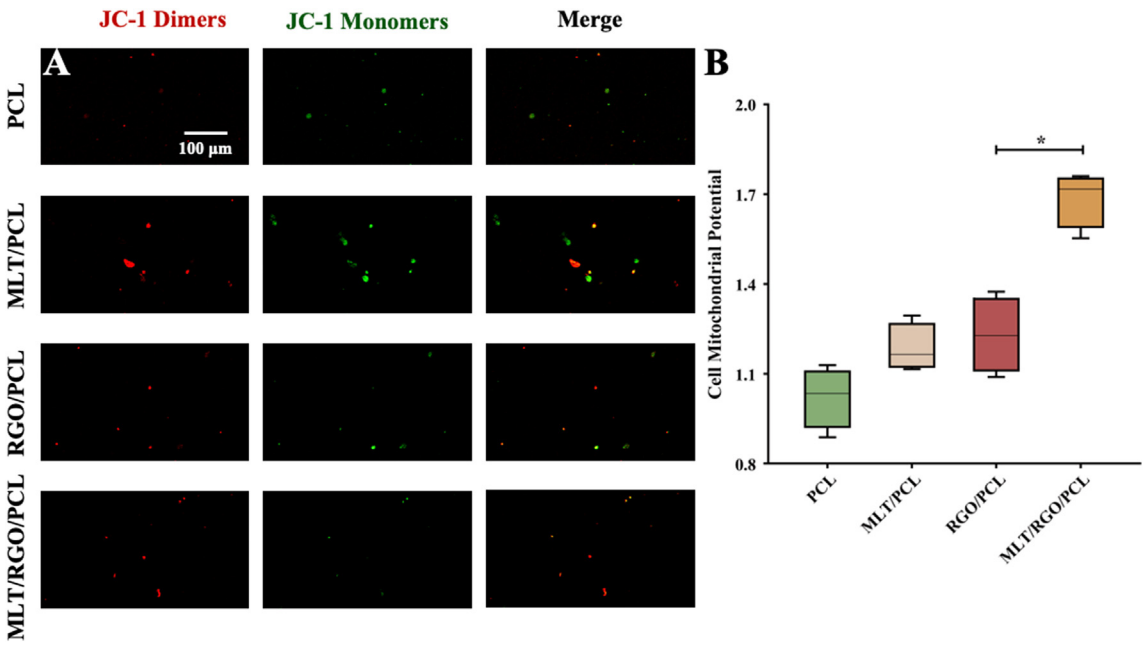

Fig. 3. Cell mitochondrial potential testing in vitro. (A,B) Mitochondrial potential of RSC 96 on PCL, MLT/PCL, RGO/PCL, and MLT/RGO/PCL scaffolds by JC-1 mitochondrial membrane potential assay, n = 4, *p < 0.05.

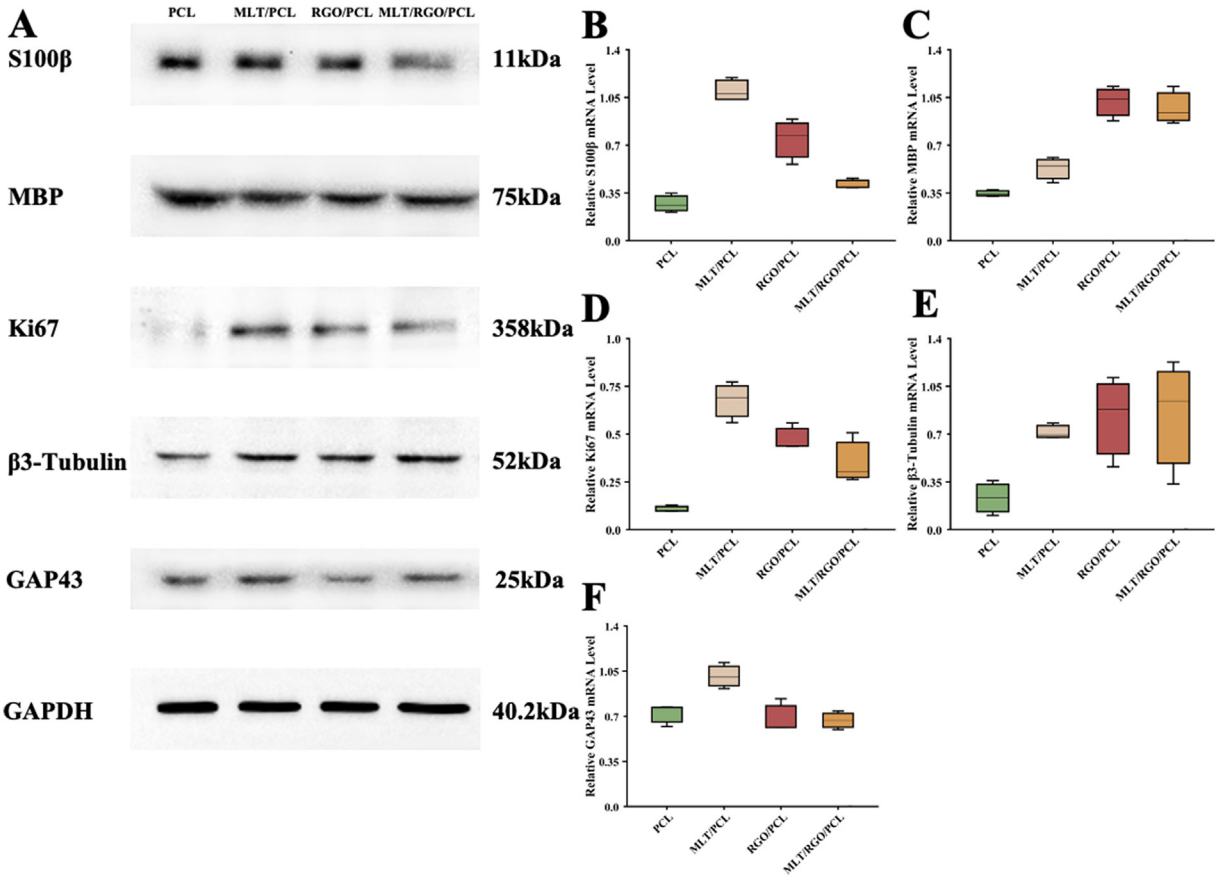

Fig. 4. Western blotting and qPCR results. (A) S100β, MBP, Ki67, β3-Tubulin, and GAP43 expression of RSC 96 on PCL, MLT/PCL, RGO/PCL, and MLT/RGO/PCL scaffolds. (B–F) Relative mRNA expression compared with GAPDH, n = 3, *p < 0.05.

0.05), and MLT/RGO/PCL scaffolds have higher cell viability than other scaffolds at 5 and 7 d ($p < 0.05$). These results showed that the scaffolds loaded with MLT or/and RGO were beneficial for cell proliferation, especially the MLT/RGO/PCL scaffolds.

The mitochondrial potential of RSC 96 was measured by the JC-1 Mitochondrial Membrane Potential Assay Kit (MCE, China). RSC 96

were cultured on PCL, MLT/PCL, RGO/PCL, and MLT/RGO/PCL scaffolds at the density of 1000 cells/cm^2 for 24 h, and images were observed under a laser scanning confocal microscopy (TCS SP8 STED 3X, China). JC-1 aggregated in the mitochondrial matrix to form JC-1 dimers of red fluorescence indicated the high mitochondrial potential of cells (Fig. 3A). On the contrary, JC-1 monomers with low mitochondrial potential were observed as green fluorescence. The mitochondrial depolarization of RSC 96 on MLT/RGO/PCL scaffolds was significantly less than other scaffolds ($p < 0.05$) (Fig. 3B). RSC 96 showed higher cell viability on MLT/RGO/PCL scaffolds.

3.3. Neural markers assay In vitro

The cell proliferation and attachment of cells were also tested by Western Blotting and qPCR. RSC 96 were cultured on the PCL, MLT/PCL, RGO/PCL, and MLT/RGO/PCL scaffolds at the density of 1×10^5 cells/cm^2 for 4 days. We measured the expression of several neural markers to test cell growth and proliferation for axonal extension both on protein and mRNA level (Fig. 4).

3.4. NGCs implantation and toxicity effect in vivo

We then implanted the PCL, MLT/PCL, RGO/PCL, and MLT/RGO/PCL conduits in 10 mm rat sciatic nerve defect models to evaluate their effect on nerve regeneration ($n = 5$). No inflammation or death occurred after animal surgery, and no collapse of conduit was observed. The toxicity effect of MLT and RGO was tested over 8 weeks in vivo. The hematoxylin-eosin (HE) staining showed that no remarkable morphological change was observed in the heart, liver, spleen, lung, and kidney of all rats. It indicated the nontoxicity of these conduits in vivo (Supplementary Fig. 3).

3.5. Immunofluorescent staining of regenerated nerve

The regenerated nerves were observed that bridged the stumps successfully when re-exposed. Ki67 is a nuclear protein that indicates cell

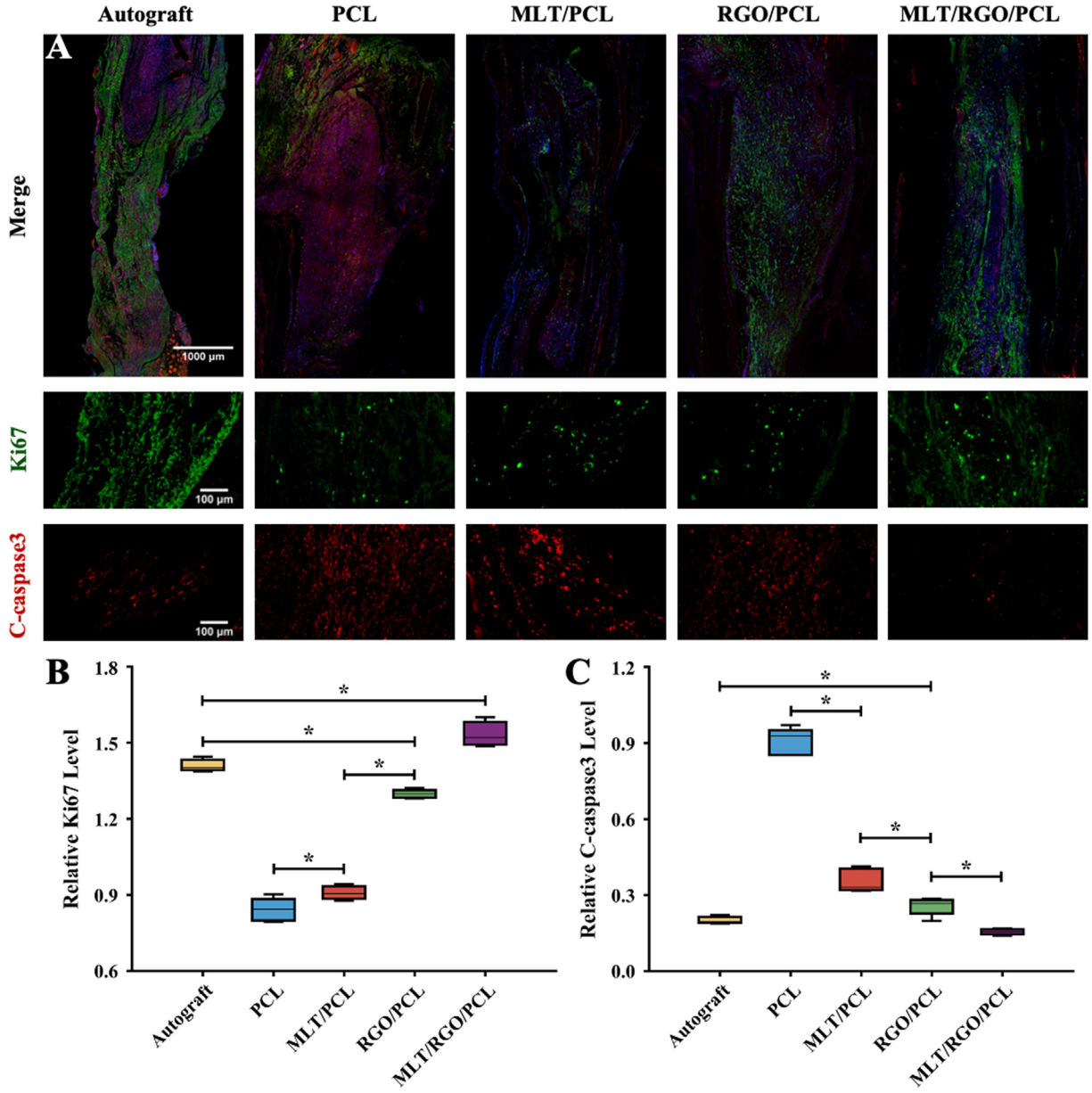

Fig. 5. Cell proliferation and apoptotic state evaluation of five groups by immunofluorescent staining at 8 weeks after surgery. (A) Immunofluorescent staining images of Ki67 (Green), C-caspase-3 (Red), and nuclei (Blue). (B) Relative level of Ki67 (Green). (C) Relative level of C-csaspase-3 (Red). The results of relative level are mean values ± SD, $n = 5$, $^*p < 0.05$.

proliferation. The relative level of Ki67 immunofluorescent staining showed a significantly higher proliferation state of axons in the MLT/RGO/PCL group than autograft group ($p < 0.05$) (Fig. 5A and B). However, the proliferation levels of the MLT/PCL and RGO/PCL groups were significantly lower than the autograft group and higher than the PCL group ($p < 0.05$). The result suggested that the addition of MLT and RGO together enhanced the axonal extension.

We evaluated the apoptotic state of regenerated nerves by C-caspase-3 immunofluorescent staining (Fig. 5A). The expression of C-caspase-3 immunofluorescent staining was exceedingly low in MLT/RGO/PCL, RGO/PCL, MLT/PCL, and autograft group (Fig. 5C). Higher C-caspase-3 expression level in the PCL group was observed than that in other groups ($p < 0.05$), and significantly lower apoptotic expression in MLT/RGO/PCL and autograft group ($p < 0.05$). These also showed the superiority of MLT/RGO/PCL to enhance cell proliferation and reduce apoptosis.

S100β is a marker of SCs commonly used for the assessment of glial cell expression. The expression level of S100β in the MLT/RGO/PCL group was significantly higher than in other groups ($p < 0.05$), which also suggested that the addition of MLT and RGO together enhanced SCs proliferation for axonal extension (Fig. 6A and B).

CD-3 could be found on the surface of T cell as a leukocyte antigen. We evaluated the immune state of regenerated nerves by CD-3 immunofluorescent staining (Fig. 6A). The relative expression level was significantly lower in MLT/RGO/PCL and RGO/PCL group than other groups ($p < 0.05$), especially lower than the autograft group ($p < 0.05$) (Fig. 6C). The addition of RGO promoted the recovery of the immune state after nerve defect, and MLT accelerated the recovery ($p < 0.05$).

3.6. Assay of regenerated nerve

Myelin basic protein (MBP) is a classic marker to evaluate the regeneration of myelin fiber. The immunohistochemistry staining of MBP in MLT/RGO/PCL and autograft group showed a significantly higher expression level than other groups ($p < 0.05$) (Fig. 7A and F). However,

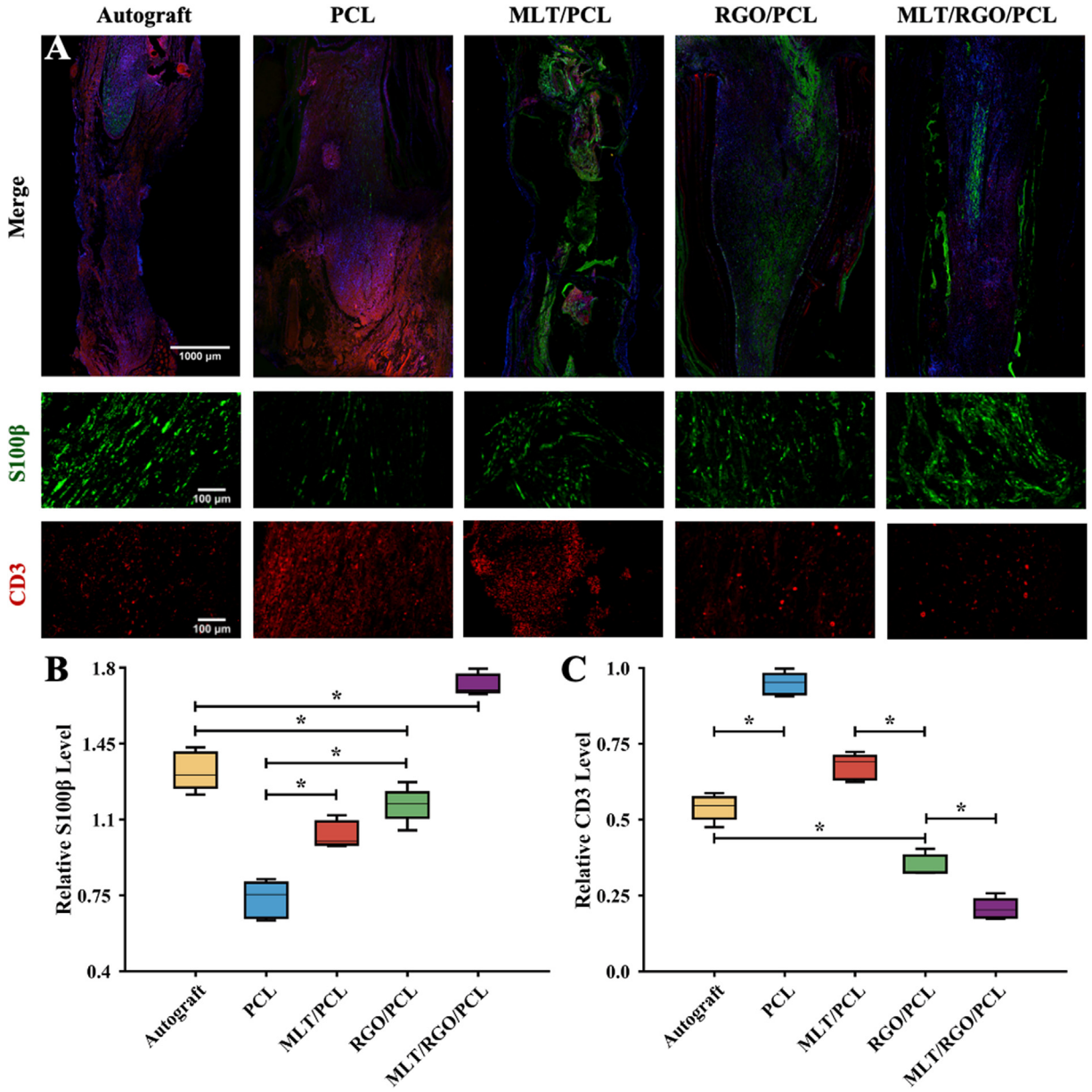

Fig. 6. Remyelination and anti-inflammation of five groups by immunofluorescent staining at 8 weeks after surgery. (A) Immunofluorescent staining images of S100β (Green), CD-3 (Red), and nuclei (Blue). (B) Relative level of S100β. (C) Relative level of CD-3 (Red). The results of relative level are mean values ± SD, n = 5, *$p < 0.05$.

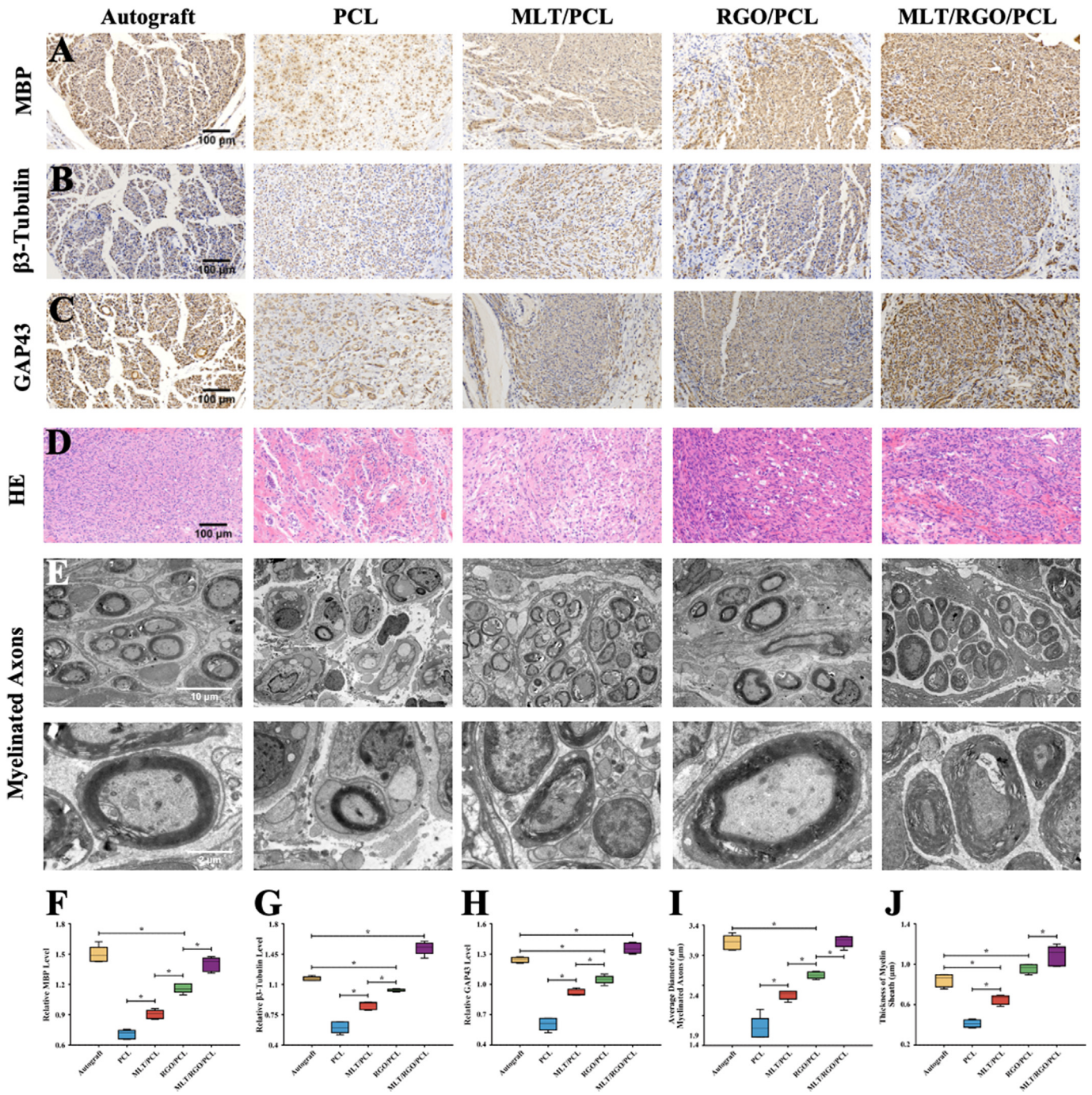

Fig. 7. Nerve Regeneration and Myelination at 8 weeks after surgery. (A) Immunohistochemistry staining images of MBP. (B) Immunohistochemistry staining images of β3-Tubulin. (C) Immunohistochemistry staining images of GAP43. (D) HE staining of regenerated nerves. (E) TEM images of myelinated axon of regenerated nerve. (F) Relative level of MBP. (G) Relative level of β3-Tubulin. (H) Relative level of GAP43. (I) Analysis of myelinated axon diameter. (J) Average thickness of myelin sheath. The results of relative level are mean values ± SD, n = 5, *p < 0.05.

there was no significance comparing MLT/RGO/PCL group to the autograft group ($p > 0.05$). The results demonstrated that MLT/RGO/PCL composite scaffolds could effectively accelerate the axonal regeneration which were similar to autograft transplantation at 8 weeks after surgery.

β3-Tubulin in neural cells is also related to the axonal extension. GAP43, also known as neuromodulin, participates in extracellular growth, synaptic development, and axon regeneration. These results revealed a similar trend in the expression of β3-Tubulin and GAP43 (Fig. 7B, C, G and H, Supplementary Fig. 4). For these two markers, the expression levels of β3-Tubulin and GAP43 in the MLT/RGO/PCL group were significantly higher than in other groups ($P < 0.05$), suggesting the better regeneration effect with the addition of MLT and RGO at 8 weeks after surgery.

HE staining and transmission electron microscopy (TEM) observations were used to evaluate myelinated regeneration. HE staining images of regenerated nerves showed that there were fewer gaps and vacuolar defects in MLT/RGO/PCL and graft group than in other groups (Fig. 7D). The denser and organized structures of nerves in the MLT/RGO/PCL

group suggested the great therapeutic effect of conduit with the addition of MLT and RGO. We measured the diameter, and thickness of myelinated axons in five groups (Fig. 7E). The diameter of myelinated axons in the MLT/RGO/PCL group had no significant differences with the autograft group ($p > 0.05$), but was significantly higher than GO/PCL, MLT/PCL, and PCL group ($p < 0.05$) (Fig. 7I). In addition, the diameter of myelinated axons in the MLT/RGO/PCL group and RGO/PCL group were remarkable higher than autograft group ($p < 0.05$), and MLT/RGO/PCL group was higher than RGO/PCL group ($p < 0.05$) (Fig. 7J). The growth of myelinated axons in the MLT/RGO/PCL group was better than the autograft group at 8 weeks after surgery.

3.7. Morphological assay of regenerated nerve

We measured the muscle fiber area to evaluate the functional regeneration of the damaged nerve because the sciatic nerve controls the gastrocnemius muscle (Supplementary Fig. 5A). The average muscle fiber area was calculated by the area of muscle fibers (Am) and the percentage of muscle fiber area (Pm). The average muscle fiber area in MLT/RGO/PCL group (85.1% ± 1.6) and graft group (81.6% ± 3.4) was much higher than in other groups ($p < 0.05$) (Supplementary Fig. 5B). The results showed that MLT/RGO/PCL conduit had a similar ability with autograft to reduce muscle atrophy ($p > 0.05$).

The electroactivity of the regenerated nerves was measured by electrophysiological tests (Fig. 8A, Supplementary Fig. 6). The nerve conducting velocity (NCV) of MLT/RGO/PCL group (34.8 ± 3.4 m/s) was significantly higher than autograft group (29.2 ± 5.6 m/s), GO/PCL group (20.3 ± 1.1 m/s), MLT/PCL group (21.8 ± 2.5 m/s), and PCL group (13.0 ± 4.4 m/s) ($p < 0.05$) (Fig. 8C). Thus, the electrophysiology was higher in MLT/RGO/PCL group than the autograft group at 8 weeks after surgery. In addition, walking tracking was used to evaluate the recovery degree of function (Fig. 8B). The sciatic function index (SFI) value of MLT/RGO/PCL group was −35.6 ± 2.2, which was significantly higher than RGO/PCL, MLT/PCL, and PCL group ($p < 0.05$) (Fig. 8D). According to the results of SFI, the autograft group (−35.2 ± 1.5) had no significant differences with MLT/RGO/PCL group ($p > 0.05$), suggesting a similar effect on functional recovery at 8 weeks after surgery.

4. Discussion

In this study, we designed an MLT/RGO/PCL composite scaffold with beaded structures for cell attachment and proliferation through electrospinning. Electrospinning is a traditional method to fabricate tissue engineering transplants and has a large number of advantages, for instance the stable topology, sizeable gap, and great mechanical properties of electrospun scaffolds for exchange of nutrient substance and cell growth in vivo. We then successfully fabricated the MLT/RGO/PCL composite scaffolds with superior mechanical properties and biocompatibility. Natural polymers such as cellulose and collagen may easily cause conduit collapse and nerve contracture [34]. In contrast, the scaffolds fabricated by PCL exhibit high mechanical properties to maintain cube structure for long-time nerve regeneration in vivo. Therefore, PCL is commonly utilized as the supporting scaffold material of tissue engineering implants [35–38].

Graphene is a type of classical two-dimensional nanomaterial with good biocompatibility and electrical conductivity [39]. The excellent biocompatibility of RGO nanomaterials and its better electrical conductivity than graphene and graphene oxide were verified by a variety of studies [40,41]. 1% (W/WPCL) RGO and 1% (W/WPCL) MLT has respectively reported that have less cytotoxicity and could promote cell adhesion and proliferation on PCL scaffolds [20,29]. Compared with PCL scaffolds, higher cell viability and mitochondrial potential of RSC 96 on

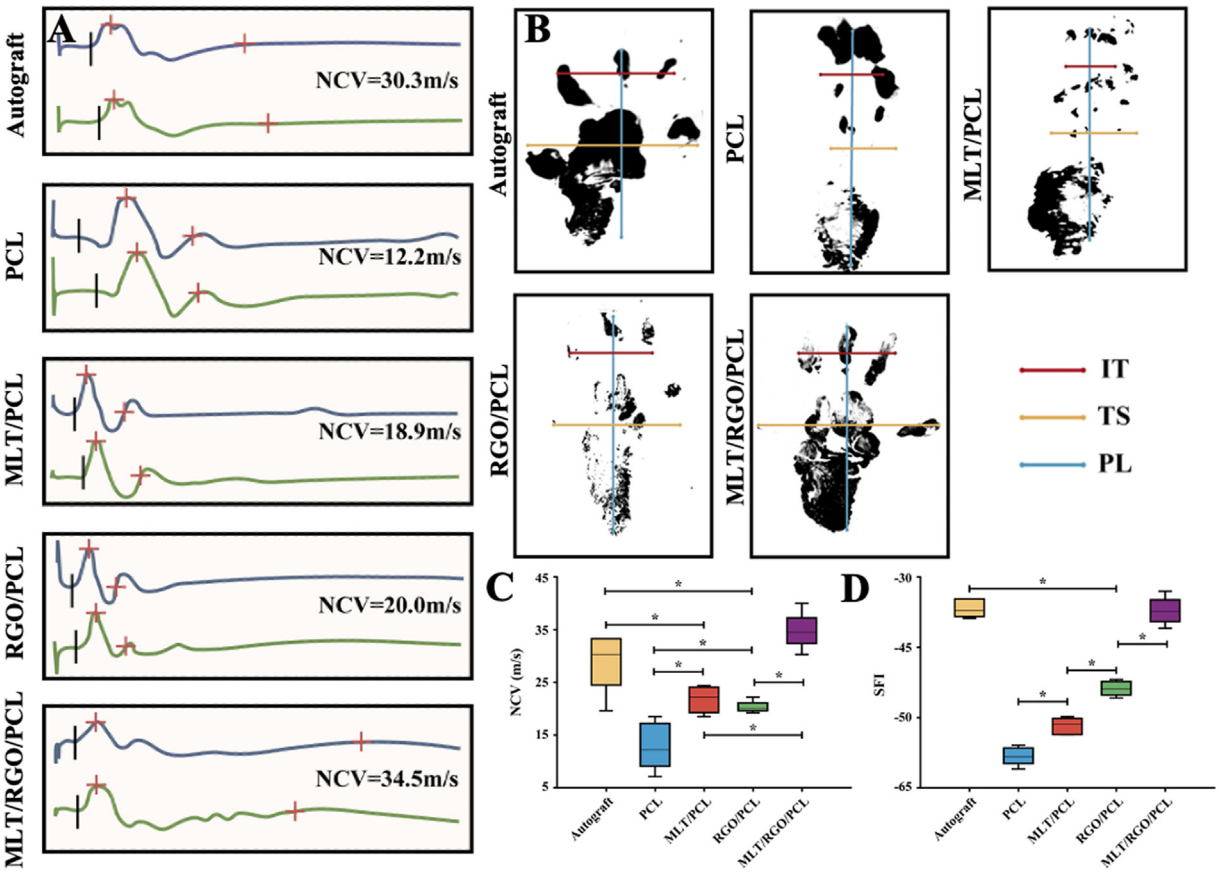

Fig. 8. Morphological assessment of regenerated nerve and distal muscle. (A) Electromyograms of regenerated nerves from the operated limb. (B) Footprints of the operated limb. (C) SFI values of regenerated nerves. (D) NCV of regenerated nerves. The results of relative level are mean values ± SD, n = 5, *$p < 0.05$.

RGO/PCL scaffolds suggested that the scaffolds could induce higher cell proliferation and attachment with the addition of RGO for peripheral nerve regeneration. A similar conclusion was reported that the RGO-coated PCL/Gelatin scaffolds enhanced the cell attachment and proliferation of embryonic neural progenitor cells seeded on them by Girão et al. [42]. The values of cell mitochondrial potential testing showed that MLT/RGO/PCL scaffold significantly improved mitochondrial function of RSCs, and the relative level is exceedingly high compared to the literature [43,44]. In addition, Carvalho et al. reported that the better mechanical properties of the scaffold were due to the addition of a variety of nanoparticles [32,33]. In this study, Young's modulus and ductility were significantly increased with the addition of RGO nanoparticles. This is very helpful to the long-term support for nerve regrowth by providing structural integrity in vivo.

Actually, electrically conductive materials could improve the growth, attachment, and differentiation of neural cells under specific electrical stimulation [45–47]. Wang et al. reported that the RGO-coated *Antheraea pernyi* silk fibroin/Poly (L-lactic acid-co-caprolactone) scaffolds accelerated nerve regeneration under electrical stimulation [48]. However, the most appropriate parameter setting of electrical stimulation device has not been reported, and electrical stimulation may cause immune rejection to the body [36].

Electrically conductive materials are considered to promote rebalance of the regenerated microenvironment as the medium for bioelectricity signal conduction [49,50]. In this study, all results from in vivo studies showed that RGO/PCL NGCs reduced the cell apoptosis and increased the cell proliferation with the higher Ki67 and lower C-caspase-3 expression levels than PCL NGCs, and accelerated the myelination and axonal outgrowth by enhancing the expression of S100β, myelin basic protein, β3-tubulin, and GAP43. These findings demonstrated the remarkable improvement of the regenerated microenvironment for peripheral nerve repair by RGO-based scaffolds.

The microenvironment imbalance after nerve defect is also induced by severe oxidative stress [51]. MLT has been demonstrated to clear free radicals in the human and animal body as classical antioxidant and anti-inflammatory chemicals [52]. With the binding to G-protein-coupled receptors MT1 and MT2, MLT expresses a variety of biological properties [18]. Stazi et al. reported that MLT could promote axonal extension via MT1 receptors for peripheral nerve regeneration [23]. In addition, MLT could activate the Wnt/β-catenin signaling pathway to promote SC migration and reduce SC apoptosis [24]. In this study, addition of MLT in the composite scaffold improved the hydrophilicity and biocompatibility of electrospun scaffolds for cell attachment and proliferation, and improved ATP synthesis for energy supply by increasing the mitochondrial potential in vitro. The immunohistochemistry staining findings showed that MLT/PCL-based composite NGCs reduced cell apoptosis with lower C-caspase-3 levels than PCL NGCs, and relevant axonal marker expression was significantly higher than PCL group in vivo. The incorporation of MLT in the scaffold helped reestablish an ideal microenvironment for peripheral nerve regeneration.

Furthermore, we fabricated a functional MLT/RGO/PCL composite scaffold to evaluate the effect in 10 mm rat sciatic nerve defect models. Of note, when performing the surgery, we inserted the proximal and distal nerve stumps into the conduit chamber for 1 mm. Therefore, the length of scaffold is 12 mm to ensure that the distance of regenerated nerve is also 10 mm. The characterization studies demonstrated that MLT and RGO improved the hydrophilicity and mechanical properties of scaffolds. The MLT/RGO/PCL scaffolds enhanced the cell attachment, proliferation, and mitochondrial potential to increase the viability of SCs seeded on the scaffolds in vitro for nerve regeneration. In in vivo study, the MLT/RGO/PCL scaffolds reduced cell apoptosis and increased its proliferation indicated by high Ki67 and low C-caspase-3 expression levels, and stimulated the myelination and axonal outgrowth by increasing relevant marker expression levels such as S100β, myelin basic protein, β3-tubulin, and GAP43. In addition, the MLT/RGO/PCL scaffolds reduced pro-inflammatory insults and accelerated the immune balance indicated by low CD-3 levels in the regenerated sciatic nerves. The expression of these markers above demonstrated that MLT/RGO/PCL scaffolds were better than RGO/PCL, MLT/PCL, and PCL scaffolds on peripheral nerve regeneration. MLT/RGO/PCL scaffolds accelerated the growth of nerve in the early stage by bioelectrical stimulation, and affected the target organ to reduce the degree of gastrocnemius muscle atrophy [31,44]. In the meantime, MLT and RGO improved axonal growth via increasing the diameter and thickness of axons, and accelerated the functional and morphological recovery of the impaired nerves.

All the results showed that the MLT/RGO/PCL composite scaffolds were beneficial to improving peripheral nerve regeneration, and the treatment effect of MLT/RGO/PCL scaffolds was close to that of autologous nerve transplanting in general at 8 weeks after peripheral nerve injury. A variety of studies demonstrated the targeted transport of drug by nanoparticles which are small enough to circulate freely throughout the body and reach the treatment sites [53–56]. Fromen et al. reported the neutrophil-nanoparticle interactions in blood circulation could drive alter neutrophil responses through the inhibition of its recruitment in acute inflammation [57]. We assumed that RGO nanoparticles released from MLT/RGO/PCL composite scaffolds delivered MLT to target treatment sites and cleared the inflammatory response of neutrophils together with MLT on peripheral nerve regeneration.

Graphene-based scaffolds will be useful clinically. The longer scaffolds implanted into the human body should require better mechanical properties, which is one of the challenges. Researchers should expend more energy on evaluating the potential mechanical properties and biocompatibility of RGO-based scaffolds in large animal models in the future before clinical practice.

5. Conclusions

In this study, the traditional electrospinning method was used to fabricate MLT/RGO/PCL composite scaffolds with excellent mechanical properties, biocompatibility, and electrical conductivity. The effects of MLT/RGO/PCL scaffolds on nerve regeneration were verified both in vitro and in vivo, and the results above demonstrated the excellent functional and morphological recovery in MLT/RGO/PCL group which were similar in autograft group at 8 weeks after nerve injury. The findings indicated the potential of MLT/RGO/PCL composite scaffolds for neural engineering applications.

Credit author statement

Huiquan Jiang, Conceptualization, Data curation, Formal analysis, Investigation, Visualization, Writing – original draft and Writing – review & editing. Xu Wang, Conceptualization, Data curation, Formal analysis, Investigation, Visualization. Xiao Li, Conceptualization, Data curation, Formal analysis, Investigation, Visualization. Yi Jin, Conceptualization, Data curation, Formal analysis, Investigation, Visualization. Zhiwen Yan, Investigation, Visualization. Xiangyun Yao, Investigation, Visualization. Wei-En Yuan, Conceptualization, Supervision, Funding acquisition, Writing – review & editing. Yun Qian, Conceptualization, Supervision, Funding acquisition, Writing – review & editing. Yuanming Ouyang, Conceptualization, Supervision, Funding acquisition, Writing – review & editing.

Declaration of competing interest

The authors declare that they have no known competing financial interests or personal relationships that could have appeared to influence the work reported in this paper.

Acknowledgements

This study was supported by the National Key R&D Program of China (No. 2021YFC2400801), the National Natural Science Foundation of

China (Nos. 82002290, 82072452 and 81830076), the Shanghai Sailing Program (No. 20YF1436000), the Natural Science Foundation of Shanghai (No. 19ZR1439200), the Municipal Hospital Newly-developing Cutting-edge Technologies Joint Research Program of Shanghai Shenkang Hospital Development Center (No. SHDC12018130), the Special Fund for Research on People's Livelihood (Medical Treatment and Public Health) of Shanghai Pudong Science, Technology and Economic Commission Scientific and Technological Development Fund (No. PKJ2018-Y52), the Shanghai Pudong Health Commission Special Program for Clinical Research in the Health Industry (No. PW2018E-01), and the Shanghai Municipal Health Commission (No. 202040399). We appreciate the support from Base for Interdisciplinary Innovative Talent Training, Shanghai Jiao Tong University and Youth Science and Technology Innovation Studio of Shanghai Jiao Tong University School of Medicine, and the help from the faculty of the Instrumental Analysis Center (IAC) of Shanghai Jiao Tong University.

Appendix A. Supplementary data

Supplementary data to this article can be found online at https://doi.org/10.1016/j.mtbio.2022.100211.

References

[1] T. Kornfeld, P. Vogt, C. Radtke, Nerve grafting for peripheral nerve injuries with extended defect sizes, Wien Med. Wochenschr. 169 (9) (2018) 240–251.
[2] W. Ray, S. Mackinnon, Management of nerve gaps: autografts, allografts, nerve transfers, and end-to-side neurorrhaphy, Exp. Neurol. 223 (1) (2010) 77–85.
[3] X. Gu, F. Ding, Y. Yang, J. Liu, Construction of tissue engineered nerve grafts and their application in peripheral nerve regeneration, Prog. Neurobiol. 93 (2) (2011) 204–230.
[4] X. Zhao, Y. Qian, Y. Cheng, X. Guo, W.-E. Yuan, One-pot construction of a twice-condensed pDNA polyplex system for peripheral nerve crush injury therapy, Biomater. Sci. 6 (8) (2018) 2059–2072.
[5] A. Nectow, K. Marra, D. Kaplan, Biomaterials for the development of peripheral nerve guidance conduits, Tissue Eng. B Rev. 18 (1) (2012) 40–50.
[6] M. Siemionow, G. Brzezicki, Chapter 8 current techniques and concepts in peripheral nerve repair, Int. Rev. Neurobiol. 87 (2009) 141–172.
[7] Y. Qian, J. Song, W. Zheng, X. Zhao, Y. Ouyang, W. Yuan, C. Fan, 3D manufacture of gold nanocomposite channels facilitates neural differentiation and regeneration, Adv. Funct. Mater. 28 (14) (2018) 1707077.
[8] S. Kehoe, X. Zhang, D. Boyd, FDA approved guidance conduits and wraps for peripheral nerve injury: a review of materials and efficacy, Injury 43 (5) (2011) 553–572.
[9] Y. Qian, Q. Han, X. Zhao, H. Li, W.-E. Yuan, C. Fan, Asymmetrical 3D nanoceria channel for severe neurological defect regeneration, iScience 12 (2019) 216–231.
[10] S. Mobini, B. Spearman, C. Lacko, C. Schmidt, Recent advances in strategies for peripheral nerve tissue engineering, Curr. Opin. Biomed. Eng. 4 (2017) 134–142.
[11] J. Zhou, Z. Hu, F. Zabihi, Z. Chen, M. Zhu, Progress and perspective of antiviral protective material, Adv. Fiber Mater. 2 (2020) 123–139.
[12] J. Hao, M. Yuan, X. Deng, Biodegradable and biocompatible nanocomposites of poly(ε-caprolactone) with hydroxyapatite nanocrystals: thermal and mechanical properties, J. Appl. Polym. Sci. 86 (3) (2002) 676–683.
[13] S.H. Oh, I. Park, J. Kim, L. Jh, In vitro and in vivo characteristics of PCL scaffolds with pore size gradient fabricated by a centrifugation method, Biomaterials 28 (9) (2007) 1664–1671.
[14] Z. Yan, Y. Qian, C. Fan, Biomimicry in 3D printing design: implications for peripheral nerve regeneration, Regen. Med. 16 (7) (2021) 683–701.
[15] Y. Qian, Y. Xu, Z. Yan, Y. Jin, X. Chen, W.-E. Yuan, C. Fan, Boron nitride nanosheets functionalized channel scaffold favors microenvironment rebalance cocktail therapy for piezocatalytic neuronal repair, Nano Energy 83 (2021) 105779.
[16] Y. Qian, W.-E. Yuan, Y. Cheng, Y. Yang, X. Qu, C. Fan, Concentrically integrative bioassembly of a three-dimensional black phosphorus nanoscaffold for restoring neurogenesis, angiogenesis, and immune homeostasis, Nano Lett. 19 (12) (2019) 8990–9001.
[17] F. Lei, M. Liang, Y. Liu, H. Huang, H. Li, H. Dong, Multi-compartment organ-on-a-chip based on electrospun nanofiber membrane as in vitro jaundice disease model, Adv. Funct. Mater. 3 (6) (2021) 383–393.
[18] R. Jockers, P. Delagrange, M. Dubocovich, R. Markus, N. Renault, G. Tosini, E. Cecon, D. Zlotos, Update on melatonin receptors. IUPHAR review: melatonin receptors, Br. J. Pharmacol. 173 (18) (2016) 2702–2725.
[19] G. Gobbi, S. Comai, Differential function of melatonin MT1 and MT2 receptors in REM and NREM sleep, Front. Endocrinol. 10 (2019) 87.
[20] Y. Xu, X. Chen, Y. Qian, H. Tang, J. Song, X. Qu, B. Yue, W.E. Yuan, Melatonin-based and biomimetic scaffold as muscle-ECM implant for guiding myogenic differentiation of volumetric muscle loss, Adv. Funct. Mater. 30 (27) (2020) 2002378.
[21] L. Manchester, A. Coto-Montes, J. Boga, L. Andersen, Z. Zhou, A. Galano, J. Vriend, D.-X. Tan, R. Reiter, Melatonin: an ancient molecule that makes oxygen metabolically tolerable, J. Pineal Res. 59 (4) (2015) 403–419.
[22] G. Ko, Circadian regulation in the retina: from molecules to network, Eur. J. Neurosci. 51 (1) (2018) 194–216.
[23] M. Stazi, S. Negro, A. Megighian, G. D'Este, M. Solimena, R. Jockers, F. Lista, C. Montecucco, M. Rigoni, Melatonin promotes regeneration of injured motor axons via MT1 receptors, J. Pineal Res. 70 (1) (2020), e12695.
[24] B. Pan, L. Jing, M. Cao, Y. Hu, X. Gao, X. Bu, Z. Li, H. Feng, K. Guo, Melatonin promotes Schwann cell proliferation and migration via the shh signalling pathway after peripheral nerve injury, Eur. J. Neurosci. 53 (3) (2020) 720–731.
[25] Y. Qian, Q. Han, X. Zhao, J. Song, Y. Cheng, Z. Fang, Y. Ouyang, W.-E. Yuan, C. Fan, 3D melatonin nerve scaffold reduces oxidative stress, inflammation and increases autophagy in peripheral nerve regeneration, J. Pineal Res. 65 (4) (2018), e12516.
[26] S. Kaplan, Effects of melatonin on peripheral nerve regeneration, recent patents on endocrine, Immune Drug Discov 5 (2) (2011) 100–108.
[27] A.K. Geim, Graphene: status and prospects, Science 324 (5934) (2009) 1530–1534.
[28] M. Gu, Y. Liu, T. Chen, F. Du, X. Zhao, C. Xiong, Y. Zhou, Is graphene a promising nano-material for promoting surface modification of implants or scaffold materials in bone tissue engineering? Tissue Eng. B Rev. 20 (5) (2014) 477–491.
[29] A. Reyad Raslan, L. Saenz Del Burgo, J. Ciriza, J. Pedraz, Graphene oxide and reduced graphene oxide-based scaffolds in regenerative medicine, Int. J. Pharm. 30 (580) (2020) 119226.
[30] M. Levin, C. Martyniuk, The bioelectric code: an ancient computational medium for dynamic control of growth and form, Biosystems 164 (2017) 76–93.
[31] Y. Qian, J. Song, X. Zhao, W. Chen, Y. Ouyang, W. Yuan, C. Fan, 3D fabrication with integration molding of a graphene oxide/polycaprolactone nanoscaffold for neurite regeneration and angiogenesis, Adv. Sci. 5 (4) (2018) 1700499.
[32] C. Carvalho, J. Silva-Correia, J. Oliveira, R.L. Reis, Nanotechnology in peripheral nerve repair and reconstruction, Adv. Drug Deliv. Rev. 148 (2019) 308–343.
[33] X. Chen, X. Ge, Y. Qian, H. Tang, J. Song, X. Qu, B. Yue, W.E. Yuan, Electrospinning multilayered scaffolds loaded with melatonin and Fe3O4 magnetic nanoparticles for peripheral nerve regeneration, Adv. Funct. Mater. 30 (38) (2020) 2004537.
[34] H. Jiang, Y. Qian, C. Fan, Y. Ouyang, Polymeric guide conduits for peripheral nerve tissue engineering, Front. Bioeng. Biotechnol. 8 (2020) 582646.
[35] J. Yan, R. Wu, S. Liao, M. Jiang, Y. Qian, Applications of polydopamine-modified scaffolds in the peripheral nerve tissue engineering, Front. Bioeng. Biotechnol. 8 (2020) 590998.
[36] Y. Cheng, Y. Xu, Y. Qian, X. Chen, Y. Ouyang, W.-E. Yuan, 3D structured Self-Powered PVDF/PCL scaffolds for peripheral nerve regeneration, Nano Energy 69 (2019) 104411.
[37] N. Siddiqui, S. Asawa, B. Birru, R. Baadhe, D.P. Sreenivasa Rao, PCL-based composite scaffold matrices for tissue engineering applications, Mol. Biotechnol. 60 (2018).
[38] L. Zhang, L. Xu, G. Li, Y. Yang, Fabrication of high-strength mecobalamin loaded aligned silk fibroin scaffolds for guiding neuronal orientation, Colloids Surf. B Biointerfaces 173 (2019) 689–697.
[39] X. Yao, Y. Qian, C. Fan, Electroactive nanomaterials in the peripheral nerve regeneration, J. Math. Chem. B 9 (35) (2021) 6958–6972.
[40] S. Zheng, L. Hao, L. Zhang, K. Wang, W. Zheng, X. Wang, X. Zhou, W. Li, L. Zhang, Tea polyphenols functionalized and reduced graphene oxide-ZnO composites for selective Pb2+ removal and enhanced antibacterial activity, J. Biomed. Nanotechnol. 14 (7) (2018) 1263–1276.
[41] X. Yao, Z. Yan, X. Wang, H. Jiang, Y. Qian, C. Fan, The influence of reduced graphene oxide on stem cells: a perspective in peripheral nerve regeneration, Regen, Biomaterials 8 (4) (2021) rbab032.
[42] A. Girão, J.P.M. Sousa, A. Dominguez-Bajo, F.A. González Mayorga, I. Bdikin, E. Pujades-Otero, N. Casañ-Pastor, M. Hortigüela, G. Otero Irurueta, A. Completo, M. Serrano, P. Marques, 3D reduced graphene oxide scaffolds with a combinatorial fibrous-porous architecture for neural tissue engineering, ACS Appl. Mater. Interfaces 12 (35) (2020) 38962–38975.
[43] Y. Gong, S. Luo, P. Fan, H. Zhu, Y. Li, W. Huang, Growth hormone activates PI3K/Akt signaling and inhibits ROS accumulation and apoptosis in granulosa cells of patients with polycystic ovary syndrome, Repord Biol. Endocrinol. 18 (1) (2020) 121.
[44] W. Liu, P. Tang, J. Wang, W. Ye, X. Ge, Y. Rong, C. Ji, Z. Wang, J. Bai, J. Fan, G. Yin, W. Cai, Extracellular vesicles derived from melatonin-preconditioned mesenchymal stem cells containing USP29 repair traumatic spinal cord injury by stabilizing NRF2, J. Pineal Res. 71 (4) (2021), e12769.
[45] Y. Qian, X. Wang, J. Song, W. Chen, S. Chen, Y. Jin, Y. Ouyang, W.-E. Yuan, C. Fan, Preclinical assessment on neuronal regeneration in the injury-related microenvironment of graphene-based scaffolds, npj Regen. Med. 6 (1) (2021) 31.
[46] Y. Qian, Y. Cheng, J. Cai, X. Zhao, Y. Ouyang, W.-E. Yuan, C. Fan, Advances in electrical and magnetic stimulation on nerve regeneration, Regen. Med. 14 (10) (2019) 969–979.
[47] Y. Qian, Y. Cheng, J. Song, Y. Xu, W.E. Yuan, C. Fan, X. Zheng, Mechano-informed biomimetic polymer scaffolds by incorporating self-powered zinc oxide nanogenerators enhance motor recovery and neural function, Small 16 (32) (2020) 202000796.
[48] J. Wang, Y. Cheng, L. Chen, T. Zhu, K. Ye, C. Jia, H. Wang, M. Zhu, C. Fan, X. Mo, In vitro and in vivo studies of electroactive reduced graphene oxide-modified nanofiber scaffolds for peripheral nerve regeneration, Acta Biomater. 84 (2018) 98–113.
[49] Y. Qian, Y. Cheng, Y. Ouyang, W.-E. Yuan, C. Fan, Multilayered spraying and gradient dotting of nanodiamond-polycaprolactone guidance channels for restoration of immune homeostasis, NPG Asia Mater. 11 (1) (2019) 36.

[50] Y. Qian, H. Lin, Z. Yan, J. Shi, C. Fan, Functional nanomaterials in peripheral nerve regeneration: scaffold design, chemical principles and microenvironmental remodeling, Mater. Today 51 (2021) 165–187.
[51] L. Zhang, K. Yao, Y. Wang, Y. Zhou, Z. Fu, G. Li, J. Ling, Y. Yang, Brain-targeted dual site-selective functionalized poly(β-amino esters) delivery platform for nerve regeneration, Nano Lett. 21 (7) (2021) 3007–3015.
[52] Y. Qian, Z. Yao, X. Wang, Y. Cheng, Z. Fang, W.E. Yuan, C. Fan, Y. Ouyang, (-)-Epigallocatechin gallate-loaded polycaprolactone scaffolds fabricated using a 3D integrated moulding method alleviate immune stress and induce neurogenesis, Cell Prolif 53 (1) (2019), e12730.
[53] V. Torchilin, Multifunctional nanocarriers, Adv. Drug Deliv. Rev. 58 (14) (2007) 1532–1555.
[54] M. Fish, A. Thompson, C. Fromen, L. Eniola-Adefeso, Emergence and utility of nonspherical particles in biomedicine, Ind. Eng. Chem. Res. 54 (2015).
[55] J. Noble, A. Zimmerman, C. Fromen, Potent immune stimulation from nanoparticle carriers relies on the interplay of adjuvant surface density and adjuvant mass distribution, ACS Biomater. Sci. Eng. 3 (4) (2017) 560–571.
[56] K. Yao, G. Gong, Z. Fu, Y. Wang, L. Zhang, G. Li, Y. Yang, Synthesis and evaluation of cytocompatible alkyne-containing poly(β-amino ester)-based hydrogels functionalized via click reaction, ACS Macro Lett. 9 (9) (2020) 1391–1397.
[57] C. Fromen, W. Kelley, M. Fish, A. Reheman, J. Noble, M. Hoenerhoff, M. Holinstat, L. Eniola-Adefeso, Neutrophil-particle interactions in blood circulation drive particle clearance and alter neutrophil responses in acute inflammation, ACS Nano 11 (11) (2017) 10797–10807.